Protein-Directed DNA Structure. I. Raman Spectroscopy of a High-Mobility-Group Box with Application to Human Sex Reversal†

James M. Benevides,‡ Ging Chan,§ Xiang-Jun Lu,|| Wilma K. Olson,|| Michael A. Weiss,*,§,⊥ and George J. Thomas, Jr*,‡

Division of Cell Biology and Biophysics, School of Biological Sciences, University of Missouri−Kansas City, Kansas City, Missouri 64110, Center for Molecular Oncology, Department of Biochemistry and Molecular Biology and Department of Chemistry, University of Chicago, Chicago, IL 60637, and Department of Chemistry, Rutgers University, New Brunswick, NJ 08903

Received January 8, 1999; Revised Manuscript Received October 29, 1999

ABSTRACT: Protein-directed reorganization of DNA underlies mechanisms of transcription, replication, and recombination. A molecular model for DNA reorganization in the regulation of gene expression is provided by the sequence-specific high-mobility-group (HMG) box. Structures of HMG-box complexes with DNA are characterized by expansion of the minor groove, sharp bending toward the major groove, and local unwinding of the double helix. The Raman vibrational signature of such DNA reorganization has been identified in a study of the SRY HMG box, encoded by the human male-determining region of the Y chromosome. We observe in the human SRY−HMG:DNA complex extraordinarily large perturbations to Raman bands associated with vibrational modes of the DNA backbone and accompanying large increases in intensities of Raman bands attributable to base unstacking. In contrast, DNA major-groove binding, as occurs for the bZIP protein GCN4 [Benevides, J. M., Li, T., Lu, X.-J., Srinivasan, A. R., Olson, W. K., Weiss, M. A., and Thomas, G. J., Jr. (2000) *Biochemistry 39*, 548−556], perturbs the Raman signature of DNA only marginally. Raman markers of minor-groove recognition in the human SRY−HMG:DNA complex are due primarily to perturbation of specific vibrational modes of deoxyribose moieties and presumably reflect desolvation at the nonpolar interface of protein and DNA. These Raman markers may be diagnostic of protein-induced DNA bending and are proposed as a baseline for comparative analysis of mutations in SRY that cause human sex reversal.

The DNA-binding domains of gene-regulatory proteins exhibit considerable diversity in structural motif, mechanism of nucleotide recognition, and extent of induced fit at the protein−nucleic acid interface (*1*−*3*). Of particular interest is the phenomenon of protein-directed bending of the double helix, which may have functional consequences at sites remote from that of protein binding (*4*). Because high-resolution structures of DNA target sites in both protein-bound and protein-free states are not generally available, we are investigating the utility of Raman spectroscopy as a probe of protein-induced changes in DNA structure.

The focus of the present study is on the high-mobility-group (HMG)[1] box of a putative transcriptional regulator encoded by the male sex-determining region of the human Y chrosomosome (hSRY). The 87-residue fragment investigated here (*5*) is closely related to the hSRY fragment investigated previously by biochemical and NMR methods (*6*, *7*). The hSRY−HMG box binds to the minor groove of its DNA target site and substantially distorts the B-DNA conformation, as depicted in Figure 1A. The mechanism in part involves the insertion of an isoleucyl side chain (Ile 13), which expands the minor groove and induces sharp bending of the double helix toward the compressed major groove (*7*, *8*). The DNA-bound protein manifests the same L-shaped α-helical fold (Figure 1B) shared by the sequence-nonspecific class of HMG proteins (*9*−*11*). In contrast, the basic leucine zipper (bZIP) protein GCN4 recognizes the major groove but induces no appreciable change in DNA conformation upon binding to an AP-1 target site, as demonstrated in the following paper in this issue (*12*). Thus, DNA complexes of the hSRY−HMG box and GCN4 represent opposite extremes of a range of protein-directed DNA reorganizations studied by Raman spectroscopy (*13*−*16*).

† Paper LXXII in the series Raman Spectral Studies of Nucleic Acids. Supported by NIH Grants GM54378 (G.J.T.), HD33462 (M.A.W.), and GM20861 (W.K.O.). M.A.W. was an American Heart Association Established Investigator and a Lucille Markey Scholar, University of Chicago.

* To whom correspondence may be addressed. (G.J.T.) Phone: (816) 235-5247. E-mail: thomasgj@umkc.edu. (M.A.W.) Phone: (216) 368-5991. E-mail: weiss@biochemistry.cwru.edu.

‡ University of Missouri−Kansas City.

§ University of Chicago.

|| Rutgers University.

⊥ Present address: Department of Biochemistry, Wood W427, Case Western Reserve School of Medicine, 10900 Euclid Avenue, Cleveland, OH 44106-4935.

[1] Abbreviations: A_{260}, absorbance at 260 nm; bp, base pair; bZIP, basic region of the leucine-zipper motif; CD, circular dichroism; FPLC, fast-protein liquid chromatography; HMG, high-mobility-group; HMQC, heteronuclear multiple quantum coherence; HSQC, heteronuclear single quantum coherence; hSRY, sex-determining region of the human Y chromosome; hSRY−HMG box, high-mobility-group box encoded by the male sex-determining region of the human Y chromosome; HTH, helix-turn-helix; MIS, Müllerian inhibiting substance; NMR, nuclear magnetic resonance; RMD, root-mean-distance; SDS, sodium dodecyl sulfate; TBP, TATA-box binding protein; UVRR, ultraviolet-resonance Raman spectroscopy.

10.1021/bi9900525 CCC: $19.00
Published on Web 12/22/1999

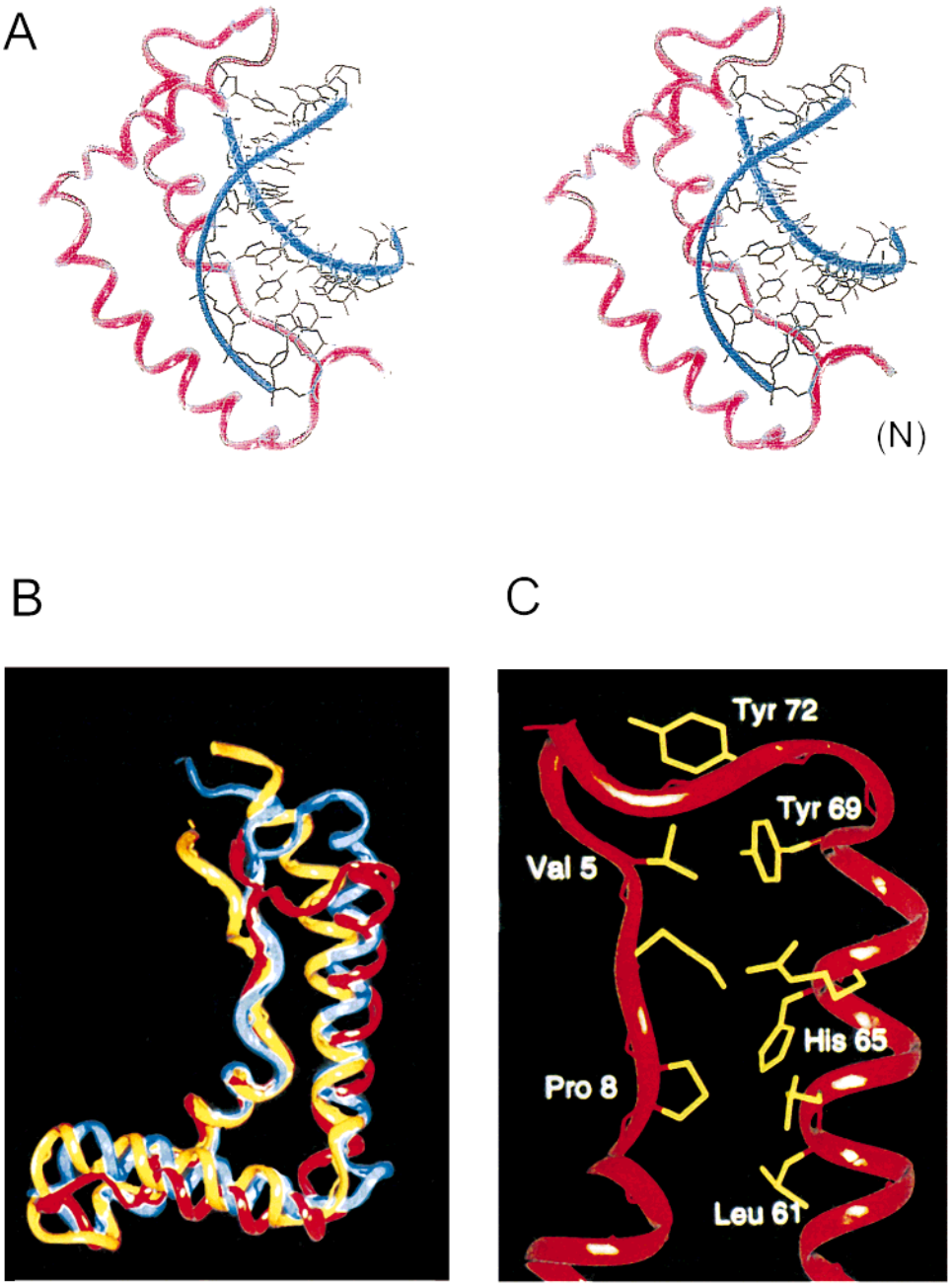

FIGURE 1: (A) Stereo model of the hSRY−HMG:DNA complex (*7*), showing paths of the protein main chain (magenta) and DNA backbone (cyan). (B) Superposition of structures of the DNA-bound hSRY−HMG box (red) and HMG boxes (yellow and blue) that bind DNA nonspecifically. (C) Packing of V5 and neighboring side chains in the minor wing of the hSRY−HMG box.

Protein-directed bending of the DNA double helix requires local backbone distortions. These are expected to perturb significantly the vibrational Raman signature of B-DNA. Although experimental and theoretical studies lend support to this hypothesis (*17*, *18*), Raman bands diagnostic of specifically bent DNA structures have not been identified. The hSRY−HMG:DNA complex may, in principle, be exploited for the purpose of identifying such Raman markers. Interest in hSRY also results from the fact that mutations in its HMG box are associated with failure of testicular differentiation leading to human sex reversal (46, XY pure gonadal dysgenesis) (*19*).

In the present study, we identify a number of unusual Raman markers specific to the native hSRY−HMG:DNA complex. Whereas complexes of major-groove-binding repressor proteins are characterized by perturbations to Raman bands of the DNA *bases* (*13*−*16*), complexes of the hSRY−HMG box are distinguished by perturbations to Raman bands associated primarily with the DNA *backbone*. The specificity of such recognition is proposed to reflect sequence-dependent backbone deformability as an example of indirect readout. We expect that the novel Raman markers identified here will be of value in the characterization of other DNA structures involved in gene regulation.

Changes in sex-specific patterns of gene expression may arise not only through loss of DNA binding but also from qualitative differences in DNA reorganization (*6*). The availability of Raman indicators of protein-induced DNA bending should provide a means of assaying such differences. As an illustration of the biomedical relevance of this

approach, we compare the Raman signature of the wild-type hSRY−HMG:DNA complex with that of the clinical variant, Val 5 → Leu (V5L), which has been implicated in pure gonadal dysgenesis (*20*, *21*). The V5L allele of hSRY has been observed in both father (an XY male) and daughter (an XY female), and so provides an example of an inherited form of sex reversal (*22*). Our results extend the repertoire of motif-specific Raman markers and have implications for the mechanism of hSRY function in gene regulation.

MATERIALS AND METHODS

1. Preparation and Purification of the hSRY-HMG Box. The present study utilizes the same 87-residue hSRY fragment investigated previously by NMR spectroscopy (sequence: G^{0} SQDRV KRPMN^{10} AFIVW SRDQR^{20} RKMAL ENPRM^{30} RNSEI SKQLG^{40} YQWKM LTEAE^{50} KWPFF QEAQK^{60} LQAMHR EKYP^{70} NYKYR PRRKA^{80} KMLPK N^{86}) (*8*). Residues Q2 through N86 of this fragment (Q57 through N141 of the human SRY protein) are numbered in accordance with the HMG-box consensus scheme defined by previous investigators (*7*, *23*). The fragment was expressed in *Escherichia coli* with a thrombin-cleavable His_6 fusion (*24*) and was purified as described (*25*). Final purification was accomplished by FPLC using a MonoS column (Pharmacia, Inc.). Purity (>98%) was assessed by SDS−polyacrylamide gel electrophoresis. The amino acid substitution V5L was introduced into the hSRY coding region in phage M13mp19RF by oligonucleotide-directed mutagenesis and polymerase chain reaction and was cloned into an expression plasmid (*24*). All constructions were verified by DNA sequencing.

2. Synthesis, Purification, and Complexation of the DNA-Binding Site. Strands of the asymmetric DNA-binding site [5′-d(GAACAATC) and 5′-d(GATTGTTC)] were synthesized on an Applied Biosystems model 381A DNA synthesizer using controlled pore glass supports and β-cyanoethyl phosphoramidite derivatives. Purification of single strands was performed on an ISCO model 2350 HPLC system, as described (*16*). Single strands were mixed in equimolar amounts on the basis of concentrations determined by UV absorbance measurements (A_{260}), brought to a final volume of 2 mL at pH 7.0, and lyophilized as duplex DNA. Approximately 0.5 mg of this duplex was resuspended in 10 mL of 50 mM KCl at pH 6.9, heated to 90 °C for 30 min, then slowly cooled to 20 °C to complete duplex annealing. Lyophilized duplex was redissolved in Milli-Q water to a concentration of 50 mg/mL, and 1:1 complexes were prepared by direct titration with hSRY−HMG, yielding the complex in 50 mM KCl at pH 7.0.

3. Raman Spectroscopy. Solutions of the hSRY−HMG box, DNA duplex, and their complex (hSRY−HMG:DNA) were sealed in glass capillary cells (Kimax no. 34507) and thermostated at 20 °C for Raman spectroscopy. Spectra were excited with the 514.5 nm line of an argon laser (Innova-70, Coherent, Inc., Santa Clara, CA) and collected on a triple spectrograph (model 1877, Spex Ind., Edison, NJ) equipped with a liquid nitrogen cooled CCD detector (model LN-CCD-1152UV, Princeton Instruments, Princeton, NJ). Usually, 10 exposures of 120 s duration were accumulated and 5−10 accumulations were averaged to produce the spectra shown below. Spectral resolution is 5 cm^{-1}. Solvent contributions to spectra were compensated by computer subtraction routines described previously (*26*). For normalization of difference spectra, the Raman band near 1092 cm^{-1}, due to the symmetric P−O stretching vibration of the phosphodioxy group (PO_2^-), was used as an internal intensity standard (*13*).

Raman difference peaks and troughs that represent at least 5% of the parent band intensity and have a signal-to-noise ratio of at least 2:1 are judged to be experimentally significant. Further discussion of Raman difference spectroscopy as a probe of structural perturbations of nucleic acids and nucleoprotein complexes is given elsewhere (*27*, *28*).

4. Conformational Analysis. DNA dimer steps from the protein/DNA complexes in the Nucleic Acid Database (*29*) and Protein Data Bank (*80*)—PDB1HRZ [35 NMR structures of the complex of SRY with the d(GTTTGTGC)·d(GCACAAAC) duplex (*7*), a slightly different sequence from the target DNA used in the current studies], PDB1LEF [12 NMR structures of the Lef-1 complex (*30*)], and PDT012 [the 1.8 Å resolution crystal structure of the yeast TATA-box binding protein complex (*31*)]—were analyzed at the backbone and base-pair level using the SCHNAaP software package (*32*). Computed torsion angles in complementary strands were compared against standard values from representative A- and B-DNA crystal structures (*33*). Dimer step parameters [Twist, Roll, and Slide (*34*)], the vertical phosphate displacement within dimer steps [Z_P, a parameter known to distinguish A- and B-helical forms (*35*)], and torsion angles were plotted as a function of chain sequence to classify and compare chain conformations.

RESULTS

1. Raman Spectroscopy of the DNA Target Site. The DNA sequence d(GAACAATC)·d(GATTGTTC) is closely related to the octanucleotide duplex investigated previously by NMR as a target of hSRY−HMG interaction (*7*). The brevity of the sequence favors spectroscopic simplicity. However, it is appropriate to address the possibility of dissociation of the octanucleotide duplex into single strands in the absence of protein binding. We assessed the stability of secondary structure of the duplex and, hence, its suitability as a target for hSRY−HMG box binding as a function of temperature using Raman and NMR methods. Raman melting profiles (data not shown) indicate $T_m = 56 \pm 2$ °C and a van't Hoff enthalpy $\Delta H \cong 75$ kcal mol^{-1} for strand dissociation (*36*). The Raman melting experiments demonstrate a duplex at the conditions employed for hSRY−HMG binding (in 50 mM KCl solution at 20 °C). This has also been confirmed by NMR measurements (M. A. Weiss, unpublished results).

The complete Raman spectrum (600−1750 cm^{-1} region) of the DNA octamer is shown in Figure 2. Raman markers at 837 and 1090 cm^{-1} are diagnostic of canonical B-DNA (*37*, *38*), and bands at 668 (dT), 681 (dG), 727 (dA), 747 (dT), and 785 (dC) identify C2′-endo/anti deoxynucleosides (*39*). This spectrum is the signature of the DNA target site and provides the basis for interpreting difference bands generated by hSRY−HMG binding (see below). Band assignments are in accordance with those given previously (*27*, *40*).

2. Raman Spectroscopy of the hSRY−HMG Box. (a) Secondary Structure. The Raman spectrum of the 87-residue hSRY−HMG box (sequence above) is shown in Figure 3.

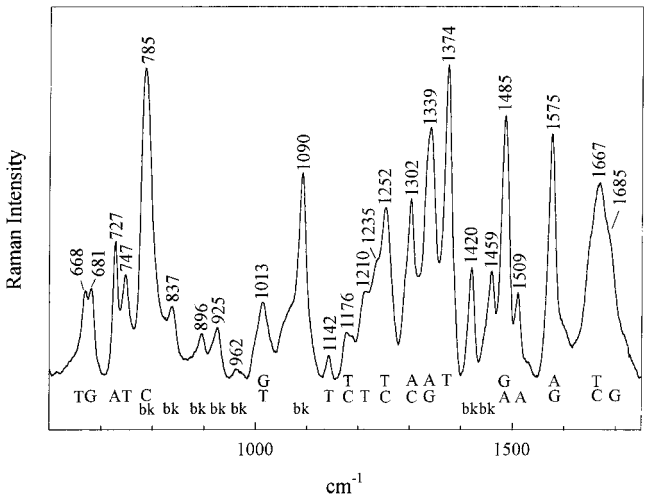

FIGURE 2: Raman spectrum in the region 600−1750 cm^{-1} of the target B-DNA sequence [d(GAACAATC)·d(GATTGTTC)] at 50 mg/mL in 50 mM KCl, pH 6.9, 20 °C. Labels indicate assignments of bands to base (C, T, A, or G) or backbone (bk) residues.

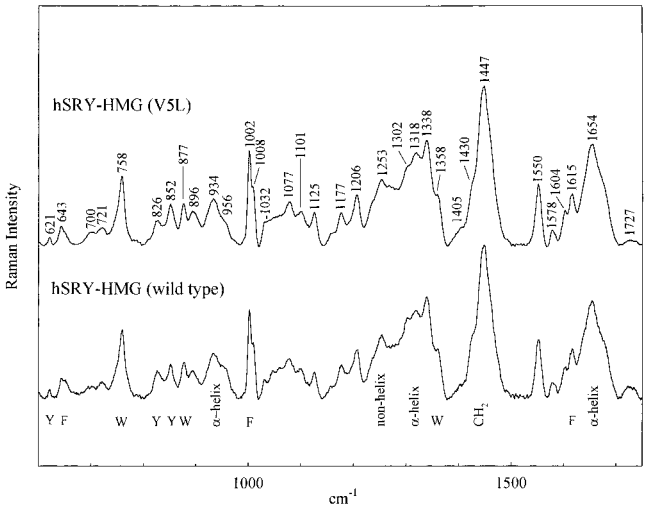

FIGURE 3: Raman spectra in the region 600−1725 cm^{-1} of the wild-type protein (hSRY−HMG box, bottom) and Val 5 → Leu mutant (hSRY−HMG^{V5L}, top), each at 50 mg/mL in 50 mM KCl, pH 7.0, 20 °C. Labels indicate Raman frequencies (cm^{-1}), amino acid assignments (one-letter abbreviations), and standard nomenclature for chemical subgroups. See also Table 1, below.

Positions of prominent amide I (peak at 1654 cm^{-1} and shoulder at 1674 cm^{-1}) and amide III bands (1302 and 1253 cm^{-1}) identify α-helix and irregular conformations as the principal types of secondary structure. The present findings are in accord with solution NMR results, indicating approximately 60% α-helix for this (and homologous) protein (*7*) and suggest further that the nonhelical regions of the protein are deficient in β-strand. This deficiency of β-strand implies that residues 1−9 of the extended N-terminal segment, which pack against helix 3 in the protein-DNA complex (Figure 1C), are not well ordered in solution in the absence of DNA binding. Such flexibility in the minor wing of the HMG box would be consistent with NMR studies of hSRY-related Sox domains (*41*, *42*).

(b) Environments of Tryptophan Side Chains. The hSRY−HMG box contains three tryptophans, Trp 15, Trp 43, and Trp 52. In the NMR structure of the specific DNA complex, the side chains of Trp 15 and Trp 43 pack in the hydrophobic core at the crux of minor- and major-wing subdomains, whereas Trp 52 projects from the back surface of the protein (*7*). The environments of these side chains in the free protein have not been characterized. Raman markers of tryptophan in the spectrum of Figure 3 report on the environment of the average Trp side chain of the free protein, as follows. The Raman band at 877 cm^{-1} (indolyl mode *W17*) indicates that the average N1H hydrogen bond is relatively strong (*43*). The structure of the DNA-bound protein provides no evidence of N1H hydrogen bonding with other protein residues, but hydrogen bonding with water molecules cannot be ruled out. Because the 877 cm^{-1} band is sharp (Figure 3), it appears that each N1H forms a relatively strong hydrogen bond. Further, the indoles exhibit a Fermi doublet with components near 1358 and 1338 cm^{-1} (*44*), for which the intensity ratio $I_{1358}/I_{1338} < 1$ is diagnostic of a hydrophilic environment for at least two and possibly all three tryptophan side chains. Finally, the sharp Raman marker at 1550 cm^{-1} (indolyl mode *W3*) indicates that the magnitude of the C2−C3−Cβ−Cα side-chain torsion angle, $|\chi^{2,1}|$, is in the low anti range (approximately 95°) for all Trp residues (*43*). Thus, Trp side-chain orientations in the free protein are very different from those in the specific complex (Trp 15, Trp 43, and Trp 52 exhibit respective $\chi^{2,1}$ values of −47°, +166°, and +42° in the NMR complex).

(c) Environments of Tyrosine Side Chains. The four tyrosines of the hSRY−HMG box, Tyr 41, Tyr 69, Tyr 72, and Tyr 74, contribute to a pair of Raman bands (Fermi doublet near 852 and 826 cm^{-1}), for which the relative intensity ratio ($I_{852}/I_{826} = 1.7$) indicates that the average phenoxyl group is a somewhat greater acceptor than donor of hydrogen bonds in the free protein (*45*). This confirms that the tyrosine phenoxyls are not all exposed to solvent. In the NMR structure of the complex, Tyr 41 projects from the surface of helix 3, whereas the remaining tyrosines occur in the C-terminal region (Figure 1C). As shown below, the average tyrosine phenoxyl environment is affected by DNA binding.

3. Raman Analysis of the Wild-Type hSRY-HMG:DNA Complex. Raman spectra of the specific complex (hSRY−HMG:DNA) and sum of constituents (hSRY−HMG + DNA) are given in the top and second-from-top traces, respectively, of Figure 4. Subtraction of the two (complex minus sum) yields the difference spectrum shown in the lower two traces of Figure 4. The large number of difference bands and their high intensities are evidence of dramatic structural rearrangements with binding. In the following sections, a structural interpretation is proposed on the basis of previously established Raman conformation markers (*17*, *39*, *46*) and available NMR results (*7*). Our focus is on identifying effects of minor-groove binding on the Raman spectrum of the DNA target site and reciprocal effects on the Raman spectrum of the bound protein.

(a) Changes to DNA Structure. (i) Raman Markers of Backbone Conformation. The spectral interval 600−900 cm^{-1}, which contains definitive Raman markers of deoxynucleoside conformation and DNA backbone geometry (*39*), exhibits large spectral perturbations with binding of the hSRY−HMG box to the DNA target site (Figure 4, bottom). The 792 cm^{-1} component of the 784/792 cm^{-1} doublet (Figure 4, top) is due to a vibration localized in phosphodiester groups of B-DNA and is diagnostic of B-form backbone geometry, specifically of torsions α and ζ in the *gauche*$^-$

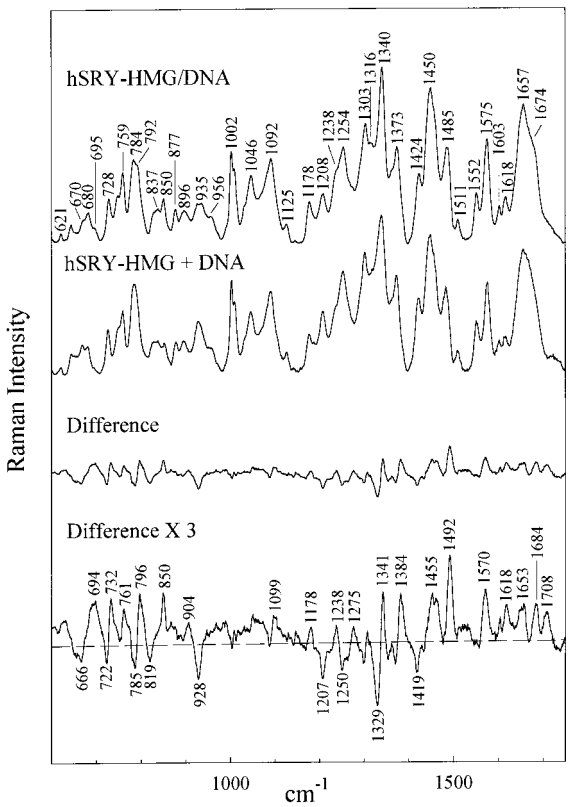

FIGURE 4: Raman spectra in the region 600−1725 cm^{-1} of the specific complex of the hSRY−HMG box with DNA (top), the spectral sum of constituents (second from top), the computed difference spectrum (complex minus sum of constituents, second from bottom), and a 3-fold amplification of the difference spectrum (bottom).

range. On protein binding, the B-form marker shifts to lower wavenumber, producing a derivative feature with peak at 796 and trough at 785 cm^{-1} in the difference spectrum. This indicates that protein binding induces a conformational change in DNA phosphodiester moieties. The structural transformation is also evidenced by other Raman band perturbations, including intensity loss at 819 cm^{-1} and concomitant gain at 850 cm^{-1}. Because the Raman band near 819 cm^{-1} is correlated with AT domains of DNA (*47*, *48*), its intensity loss implicates AT sites as direct targets of hSRY−HMG binding. Raman difference bands at 850 cm^{-1} have been observed previously in DNA structures for which the usual gauche$^-$/trans/gauche$^+$ conformation of torsions α, β, and γ, respectively, is converted to all trans (*14*−*16*, *49*, *50*). In the case of bacteriophage D108 Ner repressor, for example, the 850 cm^{-1} feature was proposed as an indicator of underwinding of the double helix (*16*).

(ii) Raman Markers of Deoxynucleoside Conformation. In addition to changes in DNA phosphodiester geometry, deoxynucleoside conformations are also altered in the complex. The troughs at 666 and 722 cm^{-1} and peak at 732 cm^{-1} in the Figure 4 difference spectrum are consistent with a change in dT conformation from C2′-endo/anti to C3′-endo/anti (*51*). Similarly, the derivative feature near 1329−1341 cm^{-1} and peak near 694 cm^{-1} indicate changes in dA and/or dG conformations. The Figure 4 difference spectrum supports previous proposals (*7*, *8*) that hSRY−HMG binding perturbs AT-paired regions of the target site.

(iii) Raman Markers of Base Environment and Interaction. Figure 4 difference peaks at 1238, 1492, and 1570 cm^{-1} are attributed to recovery of Raman hypochromism (*36*, *48*, *50*, *52*), due to base unstacking with hSRY−HMG binding. Raman bands that serve as markers of major-groove hydrogen-bonding interactions have also been described (*13*−*16*). The prototype is the guanine mode near 1490 cm^{-1}, which shifts to near 1470 cm^{-1} with N7 hydrogen bonding (*13*−*15*, *53*, *54*), producing a highly characteristic difference band profile with trough at ∼1485 cm^{-1} and peak at ∼1475 cm^{-1}. Interestingly, Figure 4 does not show such a profile. This is consistent with a minor-groove binding mechanism.

Thymine exhibits a prominent Raman band of the exocyclic $C5H_3$ group near 1376 cm^{-1} (*55*), which increases in intensity as the hydrophobicity of the $C5H_3$ environment increases (*13*). In the wild-type λ repressor/operator complex, for example, the band intensity increases due to shielding of thymine $C5H_3$ groups by the hydrophobic side chains of bound repressor (*15*). Figure 4 suggests more complicated behavior in the case of hSRY−HMG:DNA, probably involving a band shift to ca. 1384 cm^{-1} and an accompanying intensity increase. Presently, no definitive basis exists for interpreting this observation, although protein contacts (such as partial intercalation of isoleucine) may be responsible.

(iv) Raman Bands of the Deoxyribose Ring. On the basis of NMR results (*7*), it has been proposed that electrostatic and hydrophobic interactions constitute a framework to stabilize bent DNA and provide a scaffold upon which additional residue-specific contacts take place. Eleven of sixteen sugar rings are involved in such contacts. Therefore, we expect Raman bands associated with the furanose moiety to be perturbed significantly by hSRY−HMG binding. Indeed, Raman difference bands at 928, 1419, and 1455 cm^{-1} (Figure 4, bottom), assigned to the furanose ring (*17*), reflect large perturbations due to hSRY−HMG binding at deoxyribose sites. None of the affected bands is perturbed by other DNA-binding mechanisms (*12*, *15*, *16*, *46*). The band at 928 cm^{-1}, assigned to bond stretching of the deoxyribose ring (*17*), exhibits the largest perturbation, an intensity loss of about 33%. The difference bands at 1419 and 1455 cm^{-1}, assigned, respectively, to CH_2 scissoring modes of $C5'H_2$ and $C2'H_2$ groups (*17*), show that the deoxyribose structural perturbations are delocalized. Because the furanose Raman bands undergo changes in intensity without apparent changes in wavenumber, the perturbations are considered to reflect altered residue environments (hydrophobic contacts with protein) rather than altered helix geometry (such as bending and/or unwinding).

(b) Changes in Protein Structure in hSRY−HMG Complexes. Raman difference features at 761, 1099, 1178, 1207, and 1341 cm^{-1} can be attributed to reorientation and repacking of side chains of the hSRY−HMG box with DNA binding. Magnitudes of these features suggest that the number of affected side chains (∼25−30 residues) is larger than the subset of side chains (∼12) at the protein−DNA interface (*7*). In support of the Raman findings, ^{1}H NMR studies of the SRY peptide−DNA complex demonstrate unusually large complexation shifts among DNA resonances, as previously described (*8*). The resolution of eight imino resonances in the spectrum of the complex at 40 °C is in accord with the duplex status of the DNA (data not shown).

Fingerprint regions of the ^{1}H-^{15}N heteronuclear quantum coherence (HSQC or HMQC) spectra of the same hSRY−HMG box and hSRY−HMG:DNA complex analyzed by

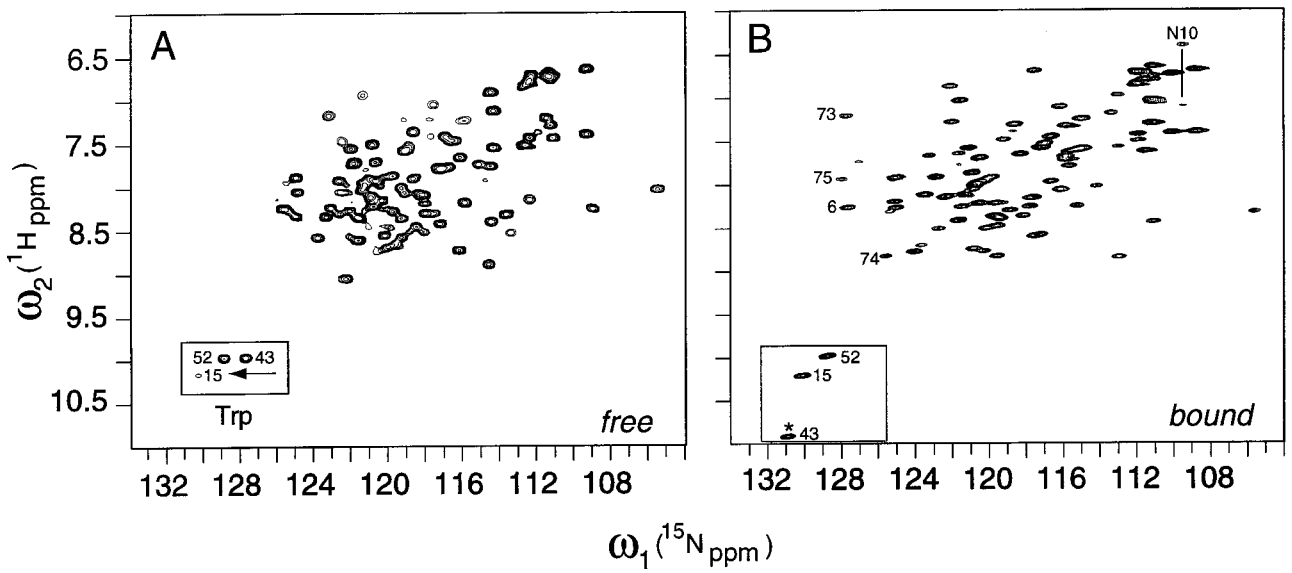

FIGURE 5: (A) ^{1}H-^{15}N HSQC spectrum of the free hSRY−HMG domain and (B) ^{1}H-^{15}N HMQC spectrum of a specific equimolar complex with the 8 bp target site. Both sequences are identical to those employed in the Raman analysis. The spectral region shown contains peptide NH "fingerprint" cross-peaks. The inset at the lower left of each panel contains the three indole NH resonances; the side-chain carboxamide resonances cluster at the upper right; the arrow in panel A indicates the anomalously broad NH resonance of Trp 15; the asterisk in panel B indicates the downfield-shifted indole resonance of Trp 43. Spectra were observed at 600 MHz in 50 mM KCl and 10 mM potassium phosphate (pH 6.5) at 25 °C in 90% H_2O and 10% D_2O. The protein concentration was 1 mM. Because the free domain exhibits large variations in NH line widths, line broadening was modulated in panel A to enhance sensitivity for broad cross-peaks of low intensity, as exemplified by the indole of Trp 15 (arrow); lower contours were also employed. Exponential apodization and low contouring is not needed in the complex, which exhibits more uniform proton line widths (panel B). Line width variation of the free domain is ascribed to conformational fluctuations on the NMR (msec) time scale; such motions are presumably damped in the complex.

Raman are shown in Figure 5 for samples uniformly enriched with ^{15}N. Unlike examples of lock-and-key ligand binding, in which complexation shifts are ordinarily localized at the macromolecular interface, the spectra of the free and bound domains exhibit little correspondence. Changes in chemical shift are observed among the majority of peptide NH resonances and thus are not confined to the 12 residues (*7*) at the protein−DNA interface. This is consistent with the Raman results. Although the protein is monomeric in the absence of DNA, it exhibits major and minor cross-peaks of variable intensity, suggesting slow and intermediate conformational exchanges. The spectrum of the bound state exhibits a single predominant conformation. With DNA binding, the indole NH resonances of the three tryptophan side chains (boxes inset in each panel) exhibit changes in both line width (narrowing of the anomalously broad Trp 15 resonance; arrow in panel A) and chemical shift (1 ppm downfield shift of the Trp 43 resonance; asterisk in panel B). No significant changes are observed in the line width and chemical shift of the Trp 52 resonance, consistent with its location on the back surface of the domain. The qualitative and quantitative changes in the HSQC spectrum of the protein suggest a nonlocal conformational adjustment of the hSRY−HMG box upon DNA binding. [A detailed description of these NMR results will be given elsewhere (E. Rivera, H. Chen, A. Radek, J. Radek, G. C., and M.A.W., manuscript in preparation).]

Despite changes in the NMR footprint of the main chain and Raman signature of side-chain environments, no significant change is observed in protein helix content upon binding, as judged by amide I and amide III markers. This implies modification (and stabilization) of tertiary structure utilizing preexisting α-helical segments. A more detailed assessment of tertiary structure, such as packing of residues 1−9 in the minor wing, cannot be assessed due to overlap of Raman bands of protein and DNA components.

4. Raman Analysis of a Mutant (V5L) hSRY−HMG:DNA Complex. An inherited form of XY sex reversal with incomplete penetrance is associated with the substitution V5L in the hSRY−HMG box (*20*, *21*). Werner et al. (*7*) speculated that C-terminal side chains of the HMG box interact more favorably with V5 than L5 in presenting an effective binding surface for DNA (Figure 1C). Nevertheless, gel assays (Supporting Information) appear to show that wild-type and V5L domains exhibit similar specific DNA-binding affinities. The decrease in binding efficiency of the variant is modest ($K_d^{V5L}/K_d^{WT} < 1.5$). We have obtained the Raman spectrum of the V5L mutant complex (hSRY−HMG^{V5L}:DNA) for comparison with the Raman signature of the wild-type complex.

The upper trace of Figure 6 shows the difference spectrum computed by subtracting the spectrum of the wild-type complex (hSRY−HMG:DNA) from that of the mutant complex (hSRY−HMG^{V5L}:DNA). Only weak Raman difference bands assignable to protein are evident, indicating that DNA structures in the mutant and wild-type complexes are very similar to one another and dramatically different from the protein-free DNA target site. A spectral subtraction showing direct comparison of the mutant complex with its constituents (available as Supporting Information) confirms the virtual identity of the perturbed DNA structures. Thus, gel assays indicating apparently similar K_d values for wild-type and mutant complexes are supported by the Raman results demonstrating overall structural similarity of the two complexes. Analogous NMR evidence suggests that structural differences are small and localized to the immediate environment of the mutated side chain (H. Chen and M.A.W.,

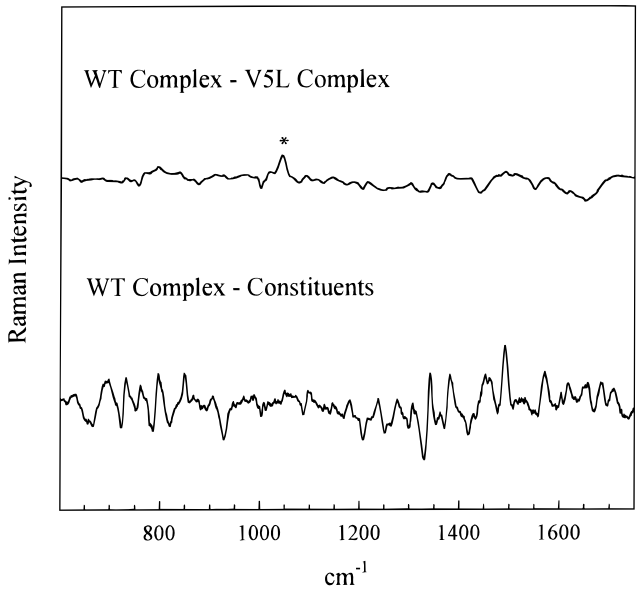

FIGURE 6: (Bottom) Raman difference spectrum (from Figure 4) demonstrating the dramatic change in structure of target DNA associated with wild-type hSRY−HMG binding. (Top) Raman difference spectrum demonstrating overall structural similarity of DNA in wild-type (hSRY−HMG:DNA, minuend) and mutant (hSRY−HMG^{V5L}:DNA, subtrahend) complexes. The difference band observed near 1045 cm^{-1} (asterisk) is due to uncompensated buffer; other weaker features are assignable to minor differences in protein content.

unpublished results). The close correspondence between DNA-specific difference features of native and variant complexes implies that the induced DNA bend angles are also similar, an inference supported directly by permutation gel electrophoresis (A. Jancso-Radek and M.A.W., unpublished results). In view of the dramatically different clinical phenotypes, similar DNA-binding and structural properties of wild-type and mutant hSRY domains are unexpected and contrast sharply with the large nonlocal structural effects shown previously to result from mutations in the λ repressor DNA-binding domain (*15*).

DISCUSSION

Sexual dimorphism provides a model of a genetic switch between alternative programs of development (*56*). The male phenotype in mammals is determined by SRY, a specific HMG-box protein and putative transcription factor encoded by the Y chromosome (*20*, *21*, *57*−*65*). Lacking discrete domains of transcriptional activation or repression, hSRY appears to function through its HMG box. The present study employs the hSRY−HMG box as a specific DNA-bending protein. Novel Raman markers are obtained (Tables 1 and 2) and utilized in the comparative study of a clinical variant associated with an inherited form of sex reversal.

1. Raman Markers of DNA Recognition. In previous papers of this series, we identified Raman difference signatures that serve as fingerprints of DNA major-groove recognition and nonspecific recognition. The former is exemplified by wild-type and mutant cI repressors of phage λ (*15*) and the Ner repressor of phage D108 (*16*); the latter is represented by the single-stranded DNA-binding protein of phage M13 (*46*). Here, we have exploited the hSRY−HMG box as a Raman model for a third mechanism of DNA binding, minor-groove recognition. An additional model of protein−DNA recogniton is furnished by the basic leucine-zipper (bZIP) motif, which is the focus of the following paper in this issue (*12*). Collectively, these results define a library of Raman markers to distinguish different modes of DNA recognition (*12*).

Table 1: Raman Frequencies, Intensities, and Assignments for the hSRY−HMG Box[a]

frequency (cm^{-1})	intensity	assignment[b]
591	0.7	M
598	0.4	(P)
621	0.5	F
643	1.3	Y
649	1.1	(M)
700	0.7	M, W, E
721	1.0	M, Y
758	4.4	W, V
826	1.7	Y
852	2.2	Y, (P,Q)
877	2.4	W
896	1.9	A, (Q)
934	3.1	skeletal mode α-helix
956	2.3	[CH_3 symmetric rock]
1002	6.0	F
1008	3.7	W
1032	1.8	F
1045	4.1	S, T (E, D) [C−O stretch]; (P) [C_α−N stretch]
1077	2.6	[C−C stretch]; K, R, Q, N [C−N stretch]
1101	1.7	P [C_α-N stretch]; [C−C stretch]
1125	1.6	W; [C−C stretch]; [C−N stretch]
1157	.8	[C−N stretch]
1177	2.2	Y, F; [CH_3 symmetric rock]
1206	1.7	Y, F
1253	4.2	amide III
1302	5.3	amide III
1318	5.8	[CH_2 twist/wag]
1338	6.7	W; [CH_2 twist/wag]
1358	3.3	W
1405	.9	[COO^- symmetric stretch]
1430	4.2	W; [CH_2, CH_3 def]
1447	10.0	[CH_2 scissor]
1550	3.8	W
1578	1.0	W, F
1604	2.1	Y, F
1615	3.4	Y, W
1654	6.7	amide I
1674	4.1	amide I
1727	1.1	(E, D, Q, N) [C═O stretch]

[a] Frequencies (cm^{-1}) units and relative intensities on an arbitrary 0−10 scale are from data of Figure 4. [b] Assignments to specific amino acid side chains (one-letter abbreviations) are based upon recent studies of isotope-labeled proteins (*74*, *76*−*79*). Square brackets ([ ]) indicate chemical-group frequencies common to more than one type of side chain.

2. Minor-Groove Recognition and Base Geometry. DNA minor-groove binding by the hSRY−HMG box generates large structural perturbations in DNA, including a bend of roughly 70−80° in the double helical axis (*7*, *22*). The present work establishes that the DNA Raman spectrum responds with extraordinarily large perturbations, which are consistent with what is known about the solution structures of the hSRY−HMG:DNA complex (*7*) and a homologous complex of Lef-1 (*30*). These exhibit unusual conformational features, which resemble somewhat those of A-DNA: underwinding with expansion of the minor groove, and compression of the major groove.

Table 2: Frequencies and Proposed Assignments for Raman Difference Bands of the hSRY−HMG:DNA Complex[a]

cm^{-1} or intensity shift[b]	residue assignment	inferred structure change
785 → 796	C5′−O−P−O−C3′	modification of B-form DNA backbone
819 → 850	O−P−O−C3′	change of α, *β*, *γ* torsions (*g*⁻*tg*⁺ to *ttt*)
668 → 640	dT	C2′-endo/anti dT to C3′-endo/anti dT
722 → 732	dA	C2′-endo/anti dA to C3′-endo/anti dA
732 ↑	dA	adenine unstacking
1238 ↑	dT	thymine unstacking
1490 ↑	dG, dA	purine unstacking
1575 ↑	dG, dA	purine unstacking
928 ↓	deoxyribose ring	altered furanose geometry (DNA bending)
1419 ↓	deoxyribose C2′H_2	altered furanose geometry (DNA bending)
1455 ↑	deoxyribose C5′H_2	altered furanose geometry (DNA bending)

[a] From data of Figure 5, bottom trace. [b] Symbols →, ↑, and ↓ indicate wavenumber shift, intensity increase, and intensity decrease, respectively.

It is of interest to compare conformational features of the DNA target bound by the hSRY−HMG box with those of DNA targets bound by two other minor-groove-binding proteins, the TATA-binding protein (TBP) and Lef-1. A quantitative analysis of structural parameters that reflect DNA bending induced by the three proteins, hSRY, Lef-1, and TBP, is represented in the left, middle, and right columns, respectively, of Figure 7. The top three rows (panels A−C) display the twist, roll, and slide, respectively, of DNA base-pair steps along the three binding sites. Panel D shows a novel parameter, Z_P, demonstrated previously (*35*) to discriminate between local A- and B-forms of DNA. The error bars (one standard deviation) in each case reflect imprecision in the NMR-derived structures.

The hSRY−HMG-bound DNA (Figure 7, left column) exhibits minimal slide, a range of roll angles, uniform untwisting or underwinding, and a marginal trend toward A-DNA phosphate positioning. The largest positive roll angles occur at two points of protein−DNA contact, made by helix 3 (asterisk) and the inserted Ile 13 (arrow). A corresponding analysis of the Lef-1 DNA-binding site reveals substantial differences in the sequence-specific pattern of structural deformations. Significant positive and negative values of slide are observed within and abutting the binding site. Large positive roll angles occur only at or near the site of side-chain insertion and not at points of contact by helix 3, with the extent of underwinding (measured by twist) being highly irregular. Further, the Z_P parameter lies almost wholly within the range expected for B-DNA. Thus, the more sharply bent Lef-1 complex exhibits less A-DNA character than the hSRY−HMG:DNA complex. It is not known whether these differences reflect (a) the lengths of oligonucleotides bound to hSRY (8 bp) and Lef-1 (15 bp), (b) the unique C-terminal basic tail bound in the major groove of the Lef-1 site, or (c) the different protocols of RMD refinements in the two studies. The last possibility arises from the inclusion of both experimental and ideal restraints with different weights in the respective empirical energy functions. It will be of interest to compare Raman markers of the hSRY and Lef-1 complexes to assess the degree of similarity between molecular vibrational perturbations in the two minor-groove complexes. A robust database of TBP:DNA crystal complexes (*31*, *66*−*71*) reveals a third pattern of base-pair geometry and Z_P values, exemplified in the right column of Figure 7 by the TBP-deformed DNA from yeast (*31*). It will also be of interest to examine the Raman signature of the TBP:DNA complex for comparison with results obtained in the present hSRY−HMG:DNA analysis.

3. Minor-Groove Recognition and Deoxynucleoside Conformation. Panels E−H of Figure 7 compare the deoxyribosyl torsions, *χ*, *δ*, *ϵ*, and *ζ*, known to distinguish helical conformations (*33*) in target DNAs. The sugars in complementary strands of the hSRY−HMG:DNA complex (left column), for example, adopt *χ* and *δ* values at the borders separating A- and B-forms (*33*), with the exception of the Ile 13 intercalation site and the 5′ end, where the sugar assumes unusual puckering. In contrast, part of the sequence strand of Lef-1:DNA (middle column) adopts the novel TATA conformation (with B-type *χ* and A-type *δ*) also found between the phenylalanyl intercalation sites in TBP:DNA (right column) (*72*), while the complementary strand undergoes a concomitant B(I) → B(II) conformational switch (*73*) with characteristic flipping of *ϵ* (C4′−C3′−O3′−P) and *ζ* (C3′−O3′−P−O5′) torsions. As in the TBP:DNA complex, the TATA-like deformations in Lef-1:DNA abut the intercalation site. The B(II) steps of the Lef-1:DNA complex, however, oppose the perturbed residues, whereas those of the TBP-bound DNA are displaced to the intercalation site bordering the DNA hairpin loop in the crystal complex. These differences should be recognizable using Raman marker bands sensitive to torsions *χ* and *ζ* (*13*, *48*).

4. Induced Fit of the hSRY−HMG Box. NMR analysis of the hSRY−HMG:DNA complex (*7*) revealed a correspondence between the structure of the DNA-bound hSRY fragment and unbound structures of HMG boxes that have the potential to bind nonspecifically (*9*−*11*). This structural correspondence (Figure 1B) originally suggested that the hSRY−HMG box provides a preformed template for DNA bending, i.e., the induced fit occurs predominantly in the DNA target rather than in the protein. Such protein-dependent reorganization of DNA would represent one extreme of a range of adaptive binding, for which the opposite extreme is represented by the GCN4 bZIP domain (*12*). Recently, this perspective has been called into question by NMR structures of the hSRY-related domains, Sox-4 and Sox-5 (*41*, *42*). The Sox structures are remarkable for flexibility in the orientation of helix 3 and positioning of the N-terminal segment relative to helices 1 and 2 at the crux of the HMG box. These features imply DNA-dependent reorganization of the protein tertiary structure.

The present study demonstrates that the overall helix content of the hSRY−HMG domain is essentially conserved upon DNA binding. Nonetheless, two observations are consistent with a model of DNA-induced protein refolding. First, the extent of change in Raman markers assigned to side chains is greater than can be accounted for by the

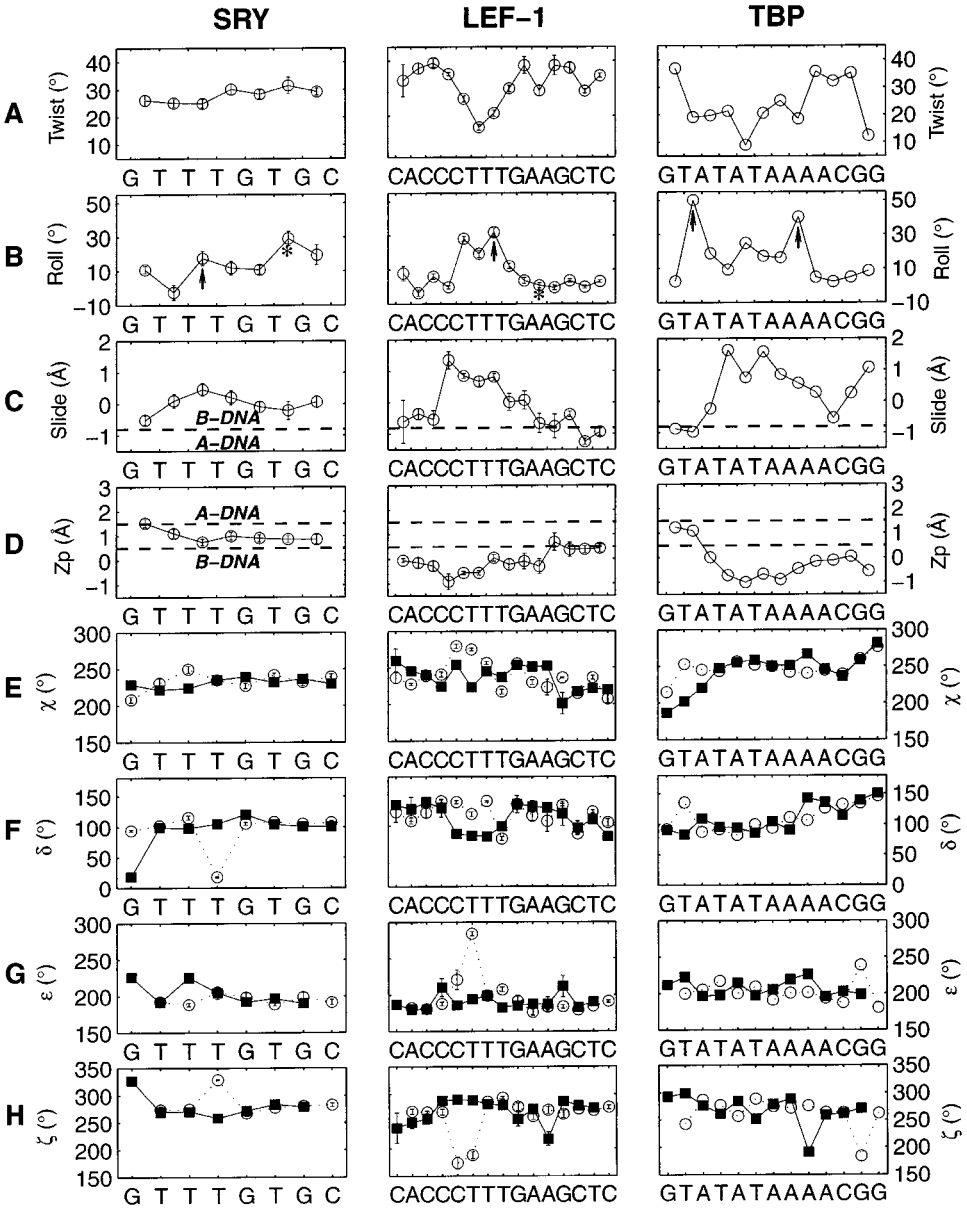

FIGURE 7: Structural comparison of the DNA associated with three minor-groove binding proteins: hSRY (left column), Lef-1 (middle column), and TBP (right column), as determined by NMR (*7*, *30*) and X-ray (*31*) methods. The respective panels (rows A−H, from top to bottom) show sequence-related variations in conformational parameters known to distinguish A- and B-DNA: local base-pair step parameters (Twist, Roll, Slide); dimer phosphate positions Z_P; and representative torsion angles (χ, δ, ϵ, and ζ), as described in the text and references therein. The vertical arrows and asterisks in the Roll plots designate amino acid intercalation sites and helix contacts, respectively. Solid squares and open circles in rows E−H distinguish torsions along the sequence strand and complementary strand, respectively. DNA from the NMR ensembles is described in terms of the averages and standard deviations (error bars) of parameters at individual base-pair steps.

number of residues in the direct protein−DNA interface, as calibrated from complexes of the λ repressor (*13*, *15*) and GCN4 bZIP protein (*12*). These difference features reflect changes in side-chain environments, not only at the hSRY−HMG−DNA interface but also in other segments (hydrophobic core) of the protein. Nonlocal changes in the HSQC NMR fingerprint of the protein on DNA binding are consistent with the Raman results. Second, Raman markers of Trp environments in the free protein in conjunction with NMR results on the complex imply alterations upon DNA binding that extend beyond the protein−DNA interface.

A prediction specific to the induced-fit Sox model (*41*, *42*) is that the N-terminal β-strand (residues 1−9) of hSRY−HMG folds against helix 3 upon DNA binding. This prediction could be tested by use of ^{13}C isotope-edited Raman spectra to resolve protein and DNA contributions in the amide I region. Such editing has been implemented in Raman studies of filamentous bacteriophage fd (*74*) and will be employed in future Raman studies of hSRY.

5. hSRY Variant and Inherited Sex Reversal. The specific affinity of the mutant HMG box (hSRY−HMG^{V5L}) for the DNA target sequence is similar to that of the wild-type HMG box (Supporting Information, Figure S1). The reduction in affinity of the variant is modest ($K_d^{V5L}/K_d^{WT} < 1.5$). This is surprising because the mutant is associated with inherited sex reversal (*20*, *21*). In addition, the mutant and wild-type complexes exhibit similar Raman band perturbations (Figure 6). It is possible that the expression and activity of hSRY are so tightly regulated in vivo that even slight reductions in affinity can disrupt testicular differentiation. Alternatively, it is possible that despite its near-native binding to naked

DNA, the variant exhibits a greater deficit in binding to in vivo targets in chromatin. Another explanation is that V5 is a site of neutral polymorphism in the human population and not a bona fide site of clinical mutation, although several observations suggest that this is not the case: First, valine is invariant at this position among both mammalian SRY alleles and autosomal Sox genes (*23*, *58*). Second, substitution of V5 has been associated with 46, XY pure gonadal dysgenesis in two independent cases of sex reversal (V5A and V5L); neither substitution is accompanied by an apparent second substitution to which the phenotype could be ascribed (*22*). Third, position 5 is variable among distinct subclasses of HMG boxes (*58*). Such a pattern of invariance within one subclass, but variability among other subclassess, suggests that the side chain participates in a subclass-specific function. The biochemical functions of hSRY in the process of testis determination are unknown. Near-native binding by the V5L variant would seem to make unlikely the hypothesis that hSRY, itself lacking an autonomous domain of transcriptional activation or repression, functions only by competitive displacement of a bona fide trancription factor (*75*).

Werner et al. (*7*) predicted that substitutions at position 5 would interfere with DNA binding by a transmitted structural perturbation. A variant interface between the N-terminal β-strand and C-terminal region (Figure 1C) could in turn affect determinants of specificity and DNA bending. A mechanism by which such perturbations could be avoided is suggested by the solution structure of hSRY-related Sox domains (*41*, *42*). As discussed above, these structures are remarkable for long-range disorder in the minor wing. In particular, the orientation of α-helix 3 relative to helices 1 and 2 is not defined, and there is no interface with the N-terminal β-strand. We propose that the hSRY−HMG box adopts a similar ensemble of structures in solution. Our results further suggest that folding of the minor wing upon DNA binding may be tolerated by a variety of mutations and without global changes in the structure of the complex. On the other hand, details of protein structure in the locus of the minor wing may be relevant to other aspects of transcription—for example, in the binding of accessory factors in a preinitiation complex. Differences in Raman spectra of the native and variant complexes suggest that such a local change in structure is necessary to accommodate the larger leucyl side chain.

CONCLUDING SUMMARY

The specific HMG box and the bZIP motif represent opposite ends of a spectrum of adaptive protein−DNA recognition. Whereas DNA provides a preformed template for the folding and assembly of GCN4 (*12*), the hSRY−HMG:DNA complex exhibits an induced fit in which protein and DNA structures adapt to one another and a dramatic reorganization of DNA structure occurs. The present study suggests that the Raman signature of the hSRY−HMG:DNA complex may serve both to identify a conserved class of minor-groove binding proteins and to discriminate subtle features of a clinical variant within this class. We propose that the difference Raman peaks at 796, 850, and 1455 cm^{-1} and the troughs at 785, 819, 928, and 1419 cm^{-1}, assignable to the DNA backbone, are due to altered normal modes of canonical B-DNA and are diagnostic of minor-groove binding (Table 2). These novel features may reflect desolvation at the nonpolar protein−DNA interface. A long-range goal of this work is to establish Raman signatures of different DNA-binding motifs. Given the importance of architectural DNA-binding proteins in mammalian embryogenesis (*6*, *56*, *60*), we anticipate that such biophysical signatures may aid in the distinction between biologically active and inactive DNA structures.

ACKNOWLEDGMENT

We thank H. Chen, A. Jancso-Radek, D. N. Jones, and L. Laboetz (U. Chicago) for assistance, Drs. J. Rose and P. E. Wright (Scripps Research Institute) for discussions and access to results prior to publication, and Drs. G. M. Clore and A. M. Gronenborn (NIH) for coordinates and restraint information on hSRY−HMG:DNA.

SUPPORTING INFORMATION AVAILABLE

Figures of a gel mobility-shift assay and a comparison of difference spectra. This material is available free of charge via the Internet at http://pubs.acs.org.

REFERENCES

1. Steitz, T. A. (1990) *Q. Rev. Biophys. 23*, 105−180.
2. Pabo, C. O., and Sauer, R. T. (1992) *Annu. Rev. Biochem. 61*, 1053−1095.
3. Patikoglou, G., and Burley, S. K. (1997) *Annu. Rev. Biophys. Biomol. Struct. 26*, 289−325.
4. Allemann, R. K., and Egli, M. (1997) *Chem. Biol. 4*, 643−650.
5. Haqq, C. M., King, C. Y., Donahoe, P. K., and Weiss, M. A. (1993) *Proc. Natl. Acad. Sci. U.S.A. 90*, 1097−1101.
6. Pontiggia, A., Rimini, R., Harley, V. R., Goodfellow, P. N., Lovell-Badge, R., and Bianchi, M. E. (1994) *EMBO J. 13*, 6115−6124.
7. Werner, M. H., Huth, J. R., Gronenborn, A. M., and Clore, G. M. (1995) *Cell 81*, 705−714.
8. King, C.-Y., and Weiss, M. A. (1993) *Proc. Natl. Acad. Sci. U.S.A. 90*, 11990−11994.
9. Weir, H. M., Kraulis, P. J., Hill, C. S., Raine, A. R. C., Laue, E. D., and Thomas, J. O. (1993) *EMBO J. 12*, 1311−1319.
10. Read, C. M., Cary, P. D., Crane-Robinson, C.-C., Driscoll, P.-C., and Norman, D. G. (1993) *Nucleic Acids Res. 21*, 3427−3426.
11. Jones, D. N. M., Searles, M. A., Shaw, G. L., Churchill, M. E. A., Ner, S. S., Keeler, J., Travers, A. A., and Neuhaus, D. (1994) *Structure 2*, 609−627.
12. Benevides, J. M., Li, T., Lu, X.-J., Srinivasan, A. R., Olson, W. K., Weiss, M. A., and Thomas, G. J., Jr. (2000) *Biochemistry 39*, 548−556.
13. Benevides, J. M., Weiss, M. A., and Thomas, G. J., Jr. (1991) *Biochemistry 30*, 5955−5963.
14. Benevides, J. M., Weiss, M. A., and Thomas, G. J., Jr. (1991) *Biochemistry 30*, 4381−4388.
15. Benevides, J. M., Weiss, M. A., and Thomas, G. J., Jr. (1994) *J. Biol. Chem. 269*, 10869−10878.
16. Benevides, J. M., Kukolj, G., Autexier, C., Aubrey, K. L., DuBow, M., and Thomas, G. J., Jr. (1994) *Biochemistry 33*, 10701−10710.
17. Thomas, G. J., Jr., Benevides, J. M., Overman, S. A., Ueda, T., Ushizawa, K., Saitoh, M., and Tsuboi, M. (1995) *Biophys. J. 68*, 1073−1088.
18. Guan, Y., and Thomas, G. J., Jr. (1996) *Biopolymers 39*, 813−835.
19. Haqq, C. M., King, C.-Y., Ukiyama, E., Falsafi, S., Haqq, T. N., Donahoe, P. K., and Weiss, M. A. (1994) *Science 266*, 453−456.
20. Berta, P., Hawkins, J. R., Sinclair, A. H., Taylor, A., Griffiths, B. L., Goodfellow, P. N., and Fellows, M. (1990) *Nature 348*, 448−450.

21. Harley, V. R., Jackson, D. I., Hextall, P. J., Hawkins, J. R., Berkovitz, G. D., Sockanathan, S., Lovell-Badge, R., and Goodfellow, P. N. (1992) *Science 255*, 453−456.
22. Hiort, O., Gramss, B., and Klaubner, G. T. (1995) *J. Pediat. 126.*, 1022.
23. Whitfield, L. S., Lovell-Badge, R., and Goodfellow, P. N. (1993) *Nature 364*, 713−715.
24. Hinck, A. P., Walkenhorst, W. F., Westler, W. M., Choe, S., and Markley, J. L. (1993) *Protein Eng. 6*, 221−227.
25. Qian, X., Gozani, S. N., Yoon, H.-S., Jeon, C., Agarwal, K., and Weiss, M. A. (1993) *Biochemistry 32*, 9944−9959.
26. Benevides, J. M., Wang, A. H.-J., van der Marel, G. A., van Boom, J. H., Rich, A., and Thomas, G. J., Jr. (1984) *Nucleic Acids Res. 12*, 5913−5925.
27. Thomas, G. J., Jr., Benevides, J. M., and Prescott, B. (1986) in *Biomolecular Stereodynamics* (Sarma, R. H., and Sarma, M. H., Eds.) pp 227−253, Adenine Press/Guilderland, New York.
28. Thomas, G. J., Jr. (1987) in *Raman Spectra and the Conformations of Biological Macromolecules* (Spiro, T. G., Ed.) pp 135−201, Wiley-Interscience, New York.
29. Berman, H. M., Olson, W. K., Beveridge, D. L., Westbrook, J., Gelbin, A., Demeny, T., Hsieh, S.-H., Srinivasan, A. R., and Schneider, B. (1992) *Biophys. J. 63*, 751−759.
30. Love, J. J. (1998) *Biophysical Characterization of the HMG-1 Box Domain of the Lymphoid Enhancer Binding Factor-1*, Ph.D. Thesis, University of California, San Diego, La Jolla, CA.
31. Kim, Y., Geiger, J. H., Hahn, S., and Sigler, P. B. (1993) *Nature 365*, 512−520.
32. Lu, X.-J., El Hassan, M. A., and Hunter, C. A. (1997) *J. Mol. Biol. 273*, 668−680.
33. Schneider, B., Neidle, S., and Berman, H. M. (1997) *Biopolymers 42*, 113−124.
34. Dickerson, R. E., Bansal, M., Calladine, C. R., Diekmann, S., Hunter, W. N., Kennard, O., von Kitzing, E., Lavery, R., Nelson, H. C. M., Olson, W. K., Saenger, W., Shakked, Z., Sklenar, H., Soumpasis, D. M., Tung, C.-S., Wang, A. H.-J., and Zhurkin, V. B. (1989) *J. Mol. Biol. 208*, 787−791.
35. El Hassan, M. A., and Calladine, C. R. (1997) *Philos. Trans. R. Soc. London A 355*, 43−100.
36. Duguid, J. G., Bloomfield, V. A., Benevides, J. M., and Thomas, G. J., Jr. (1996) *Biophys. J. 71*, 3350−3360.
37. Erfurth, S. C., Kiser, E. R., Kiser, J., and Peticolas, W. L. (1972) *Proc. Natl. Acad. Sci. U.S.A. 69*, 938−941.
38. Prescott, B., Steinmetz, W., and Thomas, G. J., Jr. (1984) *Biopolymers 23*, 235−256.
39. Thomas, G. J., Jr., and Wang, A. H.-J. (1988) *Nucleic Acids Mol. Biol. 2*, 1−30.
40. Thomas, G. J., Jr., and Tsuboi, M. (1993) *Adv. Biophys. Chem. 3*, 1−70.
41. Crane-Robinson, C., Read, C. M., Cary, P. D., Driscoll, P. C., Dragan, I., and Privalov, P. L. (1998) *J. Mol. Biol. 281*, 705−717.
42. van Houte, L. P., Chuprina, V. P., van der Wetering, M., Boelens, R., Kaptein, R., and Clevers, H. (1995) *J. Biol. Chem. 270*, 30516−30524.
43. Miura, T., Takeuchi, H., and Harada, I. (1989) *J. Raman Spectrosc. 20*, 667−671.
44. Harada, I., Miura, T., and Takeuchi, H. (1986) *Spectrochim. Acta 42A*, 307−312.
45. Siamwiza, M. N., Lord, R. C., Chen, M. C., Takamatsu, T., I., H., Matsuura, H., and Shimanouchi, T. (1975) *Biochemistry 14*, 4870−4876.
46. Benevides, J. M., Terwilliger, T. C., Vohnik, S., and Thomas, G. J., Jr. (1996) *Biochemistry 35*, 9603−9609.
47. Wartell, R. M., and Harrell, J. T. (1986) *Biochemistry 25*, 2664−2671.
48. Movileanu, L., Benevides, J. M., and Thomas, G. J., Jr. (1999) *J. Raman Spectrosc. 30*, 637−649.
49. Benevides, J. M., Wang, A. H.-J., Rich, A., Kyogoku, Y., van der Marel, G. A., van Boom, J. H., and Thomas, G. J., Jr. (1986) *Biochemistry 25*, 41−50.
50. Benevides, J. M., Stow, P. L., Ilag, L., Incardona, N. L., and Thomas, G. J., Jr. (1991) *Biochemistry 30*, 4855−4863.
51. Thomas, G. J., Jr., and Benevides, J. M. (1985) *Biopolymers 24*, 1101−1105.
52. Erfurth, S. C., and Peticolas, W. L. (1975) *Biopolymers 14* , 247−264.
53. Nishimura, Y., Tsuboi, M., Sato, T., and Akoi, K. (1986) *J. Mol. Struct. 146*, 123−153.
54. Miura, T., and Thomas, G. J., Jr. (1994) *Biochemistry 33* , 7848−7856.
55. Susi, H., and Ard, J. S. (1974) *Biochim. Biophys. Acta 312* , 311−322.
56. Lovell-Badge, R. (1993) *Philos. Trans. R. Soc. London B 339*, 159−164.
57. Sinclair, A. H., Berta, P., Palmer, M. S., Ross-Hawins, J., Griffiths, B. L., Smith, M. J., Foster, J. W., Frischauf, A. M., Lovell-Badge, R., and Goodfellow, P. N. (1990) *Nature 346*, 240−244.
58. Ner, S. S. (1992) *Curr. Biol. 2*, 208−210.
59. Cohen, D. R., Sinclair, A. H., and McGovern, J. D. (1994) *Proc. Natl. Acad. Sci. 91*, 4372−4376.
60. Goodfellow, P. N., and Lovell-Badge, R. (1993) *Annu. Rev. Genet. 27*, 71−92.
61. Koopman, P., Gubbay, J., Vivian, N., Goodfellow, P., and Lovell-Badge, R. (1991) *Nature 351*, 117−121.
62. McElreavy, K. K., Vilain, E., Abbas, N., Costa, J.-M., Souleyreau, N., Kucheria, K., Boucekkine, C., Thibaud, E., Brauner, R., Flamant, F., and Fellous, M. (1992) *Proc. Natl. Acad. Sci. U.S.A. 89*, 11016−11020.
63. Hawkins, J. R., Taylor, A., Berta, P., Levilliers, J., van der Auwera, B., and Goodfellow, P. N. (1992) *Hum. Genet. 88*, 471−474.
64. Hawkins, J. R., Taylor, A., Goodfellow, P. N., Migeon, C. J., Smith, K. D., and Berkovitz, G. D. (1992) *Am. J. Hum. Genet. 90*, 350−355.
65. Vilain, E., Jaubert, F., Fellous, M., and McElreavey, K. (1993) *Differentiation 52*, 151−159.
66. Kim, J. L., and Burley, S. K. (1994) *Nat. Struct. Biol. 1*, 638−653.
67. Kim, J. L., Nikolov, D. B., and Burley, S. K. (1993) *Nature 365*, 520−527.
68. Nikolov, D. B., Chen, H., Halay, E. D., Hoffmann, A., Roeder, R., and Burley, S. K. (1996) *Proc. Natl. Acad. Sci. U.S.A. 93*, 4862−4867.
69. Nikolov, D. B., Chen, H., Halay, E. D., Usheva, A. A., Disatake, K., Lee, D. K., Roeder, R. G., and Burley, S. K. (1995) *Nature 377*, 119−128.
70. Tan, S., Hunziker, Y., Sargent, D. F., and Richmond, T. J. (1996) *Nature 381*, 127−134.
71. Juo, Z. S., Chiu, T. K., Lieberman, P. M., Baikalov, I., Berk, A. J., and Dickerson, R. E. (1996) *J. Mol. Biol. 261*, 239−254.
72. Guzikevich-Guerstein, G., and Shakked, Z. (1996) *Nat. Struct. Biol. 3*, 32−37.
73. Grzeskowiak, K., Yanagi, K., Privé, G. G., and Dickerson, R. E. (1991) *J. Biol. Chem. 266*, 8861−8883.
74. Overman, S. A., and Thomas, G. J., Jr. (1998) *Biochemistry 37*, 5654−5665.
75. Graves, J. A. M. (1996) *Nat. Genet. 16*, 114−115.
76. Aubrey, K. L., and Thomas, G. J., Jr. (1991) *Biophys. J. 60*, 1337−1349.
77. Overman, S. A., and Thomas, G. J., Jr. (1995) *Biochemistry 34*, 5440−5451.
78. Overman, S. A., and Thomas, G. J., Jr. (1998) *J. Raman Spec. 29*, 23−29.
79. Overman, S. A., and Thomas, G. J., Jr. (1999) *Biochemistry 38*, 4018−4027.
80. Bernstein, F. C., Koetzle, T. F., Williams, G. J., Meyer, E. E., Jr., Brice, M. D., Rodgers, J. R., Kennard, O., Shimanouchi, T., and Tasumi, M. (1977) *J. Mol. Biol. 112*, 535−542.

BI9900525